Acknowledgments

The authors would like to express our appreciation to reviewers, Editors and Editorial assistant of Radiological Physics and Technology for their invaluable advice to improve our manuscript. This study was supported by a grant for research on Advanced Medical Technology from the Ministry of Health, Labour and Welfare, Japan. We would like to thank the VPL released by AZE Ltd. (Tokyo, Japan) and the software library by the Oxford University Centre for Functional MRI of the Brain. We are grateful to the staffs at the National Cardiovascular Center for their invaluable contribution and efforts. Last but not least, our thanks go to Miss Atra Ardekani (a summer intern from McGill University in Montreal, Quebec, Canada).

References

1. Brockmann MA, Kemmling A, Groden C. Current issues and perspectives in small rodent magnetic resonance imaging using clinical MRI scanners. Methods. 43. 79-87 (2007)

2. Smith DA, Clarke LP, Fiedler JA, Murtagh FR, Bonaroti EA, Sengstock GJ, et al. Use of a Clinical MR Scanner for Imaging the Rat Brain. Brain Res Bull. 31(1-2). 115-20 (1993)

3. Guzman R, Lövblad KO, Meyer M, Spenger C, Schroth G, Widmer HR. Imaging the rat brain on a 1.5 T clinical MR-scanner. J Neurosci Methods. 97(1). 77-85 (2000)

4. Fujioka M, Taoka T, Matsuo Y, Hiramatsu KI, Sakaki T. Novel Brain Ischemic Change on MRI: Delayed Ischemic Hyperintensity on T_1-Weighted Images and Selective Neuronal Death in the Caudoputamen of Rats After Brief Focal Ischemia. Stroke. 30(5). 1043-1046 (1999)

5. Thorsen F, Ersland L, Nordli H, Enger PO, Huszthy PC, Lundervold A, et al. Imaging of experimental rat gliomas using a clinical MR scanner. J. Neurooncol. 63(3). 225-231 (2003)

6. Biswas J, Nelson CB, Runge VM, Wintersperger BJ, Baumann SS, Jackson CB, et al. Brain Tumor Enhancement in Magnetic Resonance Iimaging: Comparison of Signal-to-Noise Ratio (SNR) and Contrast-to-Noise Ratio (CNR) at 1.5 Versus 3 Tesla. Invest Radiol. 40. 792-797 (2005)

7. Shimamura M, Sato N, Sata M, Kurinami H, Takeuchi D, Wakayama K, et al. Delayed Postischemic Treatment With Fluvastatin Improved Cognitive Impairment After Stroke in Rats. Stroke. 38. 3251-3258 (2007)

8. Lee JM, Zhai G, Liu Q, Gonzales ER, Yin K, Yan P, et al. Vascular Permeability Precedes Spontaneous Intracerebral Hemorrhage in Stroke-Prone Spontaneously Hypertensive Rats. Stroke. 38. 3289-3291 (2007)

9. Wintersperger BJ, Runge VM, Biswas J, Reiser MF, Schoenberg SO. Brain Tumor Enhancement in MR Imaging at 3 Tesla: Comparison of SNR and CNR Gain Using TSE and GRE Techniques. Invest Radiol. 42. 558-563 (2007)

10. Sato H, Enmi J, Teramoto N, Hayashi T, Yamamoto A, Tsuji T, et al. Comparison of Gd-DTPA-Induced Signal Enhancements in Rat Brain C6 glioma among Different Pulse Sequences in 3-Tesla Magnetic Resonance Imaging. Acta Radiol. 49. 172-179 (2008)

11. Yang YM, Feng X, Yao ZW, Tang WJ, Liu HQ, Zhang L. Magnetic resonance angiography of carotid and cerebral arterial occlusion in rats using a clinical scanner. J Neurosci Methods. 167(2). 176-83 (2008)

12. Rosen BR, Belliveau JW, Vevea JM, Brady TJ. Perfusion imaging with NMR contrast agents. Magn Reson Med. 14(2). 249-265 (1990)

13. Calamante F, Thomas DL, Pell GS, Wiersma J, Turner R. Measuring Cerebral Blood Flow Using Magnetic Resonance Imaging Techniques. J Cereb Blood Flow Metab. 19(7). 701-35 (1999)

14. Yamada K, Wu O, Gonzalez RG, Bakker D, Østergaard L, Copen WA, et al. Magnetic Resonance Perfusion-Weighted Imaging of Acute Cerebral Infarction:

Effect of the Calculation Methods and Underlying Vasculopathy. Stroke. 33(1). 87-94 (2002)

15. Tamura H, Hatazawa J, Toyoshima H, Shimosegawa E, Okudera T. Detection of Deoxygenation-Related Signal Change in Acute Ischemic Stroke Patients by T2*-Weighted Magnetic Resonance Imaging. Stroke. 33(4). 967-971 (2002)

16. Calamante F, Gadian DG, Connelly A. Quantification of Perfusion Using Bolus Tracking Magnetic Resonance Imaging in stroke: Assumptions, Limitations, and Potential Implications for Clinical Use. Stroke. 33(4). 1146-1151 (2002)

17. Latchaw RE, Yonas H, Hunter GJ, Yuh WT, Ueda T, Sorensen AG, et al. Guidelines and Recommendations for Perfusion Imaging in Cerebral Ischemia: A Scientific Statement for Healthcare Professionals by the Writing Group on Perfusion Imaging, From the Council on Cardiovascular Radiology of the American Heart Association. Stroke. 34(4). 1084-1104 (2003)

18. Carroll TJ, Rowley HA, Haughton VM. Automatic Calculation of the Arterial Input Function for Cerebral Perfusion Imaging with MR imaging. Radiology. 227(2). 593-600 (2003)

19. Wintermark M, Sesay M, Barbier E, Borbély K, Dillon WP, Eastwood JD, et al. Comparative Overview of Brain Perfusion Imaging Techniques. Stroke. 36(9). 83-99 (2005)

20. Bruening R, Kwong KK, Vevea MJ, Hochberg FH, Cher L, Harsh GR 4th, et al. Echo-Planar MR Determination of Relative Cerebral Blood Volume in Human Brain Tumors: T1 versus T2 Weighting. AJNR Am J Neuroradiol. 17(5). 831-840 (1996)

21. Chen F, Suzuki Y, Nagai N, Peeters R, Coenegrachts K, Coudyzer W, et al. Visualization of Stroke with Clinical MR Imagers in Rats: A Feasibility Study. Radiology. 233. 905-911 (2004)

22. Chen F, Suzuki Y, Nagai N, Sun X, Coudyzer W, Yu J, et al. Delayed perfusion phenomenon in a rat stroke model at 1.5 T MR: An imaging sign parallel to spontaneous reperfusion and ischemic penumbra? Eur J Radiol. 61. 70-78 (2007)

23. Fan G, Zang P, Jing F, Wu Z, Guo Q. Usefulness of Diffusion/Perfusion-weighted MRI in Rat Gliomas: Correlation With Histopathology. Acad Radiol. 12(5). 640-651 (2005)

24. van Osch MJ, van der Grond J, Bakker CJ. Partial volume effects on arterial input functions: shape and amplitude distortions and their correction. J Magn Reson Imaging. 22(6). 704-709 (2005)

25. Wada Y, Hara T, Miyati T. Basic Assessment of the CNR Measurement Method of MRI System in Phantom-Suggestion for Improvement in the CNR Evaluation Method. Nippon Hoshasen Gijutsu Gakkai Zasshi. 64(2). 268-76 (2008)

26. Ogura A, Maeda F, Miyai A, Hongoh T. Accuracy of Contrast-to-noise Ratio Measurement for Magnetic Resonance Clinical Images. Nippon Hoshasen Gijutsu Gakkai Zasshi. 60(11). 1543-1549 (2004)

27. Miyati T. Image quality assessment in magnetic resonance imaging. Nippon Hoshasen Gijutsu Gakkai Zasshi. 58(1). 40-48 (2002)

28. Wu O, Ostergaard L, Weisskoff RM, Benner T, Rosen BR, Sorensen AG. Tracer Arrival Timing-Insensitive Technique for Estimating Flow in MR Perfusion-Weighted Imaging Using Singular Value Decomposition With a Block-Circulant Deconvolution Matrix. Magn Reson Med. 50. 164-174 (2003)

29. Besselmann M, Liu M, Diedenhofen M, Franke C, Hoehn M. MR angiographic investigation of transient focal cerebral ischemia in rat. NMR Biomed. 14(5). 289-296 (2001)

30. Bloom AS, Tershner S, Fuller SA, Stein EA. Cannabinoid-Induced Alterations in Regional Cerebral Blood Flow in the Rat. Pharmacol Biochem Behav. 57(4). 625-631 (1997)

31. Shockley RP, LaManna JC. Determination of rat cerebral cortical blood volume changes by capillary mean transit time analysis during hypoxia, hypercapnia and hyperventilation. Brain Res. 454(1-2). 170-178 (1998)

32. Meier P, Zierler KL. On the Theory of the Indicator-Dilution Method for Measurement of Blood Flow and Volume. J Appl Physiol. 6. 731-744 (1954)

33. Johansson E, Månsson S, Wirestam R, Svensson J, Petersson JS, Golman K, Ståhlberg F. Cerebral Perfusion Assessment by Bolus Tracking Using Hyperpolarized 13C. Magn Reson Med. 51(3). 464-472 (2004)

34. Enmi J, Hayashi T, Watabe H, Moriwaki H, Yamada N, Iida H. Measurement of cerebral blood flow with dynamic susceptibility contrast MRI and comparison with O-15 positoron emission tomography. Quantitation in Biomedical Imaging with PET and MRI. ICS 1265. 150-158 (2004)

35. Calamante F, Vonken EJ, van Osch MJ. Contrast Agent Concentration Measurements Affecting Quantification of Bolus-Tracking Perfusion MRI. Magn Reson Med. 58. 544-553 (2007)

36. Grandin CB, Bol A, Smith AM, Michel C, Cosnard G. Absolute CBF and CBV measurements by MRI bolus tracking before and after acetazolamide challenge: Repeatability and comparison with PET in humans. Neuroimage. 26. 525-535 (2005)

37. Kuhl CK, Träber F, Schild HH. Whole-Body High-Field-Strength (3.0-T) MR Imaging in Clinical Practice. Part I. Technical Considerations and Clinical Applications. Radiology. 246(3). 675-696 (2008)

38. Jezzard P, Clare S. Sources of distortion in Functional MRI Data. Hum Brain Mapp. 8(2-3). 80-85 (1999)

39. Mayer D, Zahr NM, Adalsteinsson E, Rutt B, Sullivan EV, Pfefferbaum A. In vivo fiber tracking in the rat brain on a clinical 3T MRI system using a high strength insert gradient coil. Neuroimage. 35(3). 1077-1085 (2007)

40. Graf H, Martirosian P, Schick F, Grieser M, Bellemann ME. Inductively coupled rf coils for examinations of small animals and objects in standard whole-body MR scanners. Med. Phys. 30(6). 1241-1245 (2003)

Figure Captions

Figure.1

The head fixation system for small animals, fitted with an MRI coil for RF transmission and reception. The coil is typically a three-turn solenoid; it can also be a single-turn coil, as shown on the top left of this figure.

Figure 2

T_1-W images (top) and T_2-W images (bottom) obtained from an SD rat, with the following anatomic locations as indicated: the somato-sensory cortex (SS), corpus callosum (CC), parietal cortex (Pt), external capsule (EC), caudate putamen (CPu), internal capsule (IC), hippocampus (HC), thalamus (Thal), auditory cortex (Au), amygdala (AM), hypothalamus (HT), internal carotid arterial system (ICAs), trigeminal nerve (TN), interpeduncular cistern (IPC), dorsal third ventricle (D3V), and the lateral ventricle (LV). These slice sections resemble the distance of -1.5 mm (left) and -3.5 mm (right), respectively, in appearance from the Bregma.

Figure 3

Partial maximum-intensity-projection maps of contrast-free time-of-flight MRA obtained for a Sprague-Dawley rat. Maps represent areas around the Thal (A), right hemisphere (B), and left hemisphere (C).

Note: the white arrows indicate the selected ROI level (as described in the Discussion). AZACA: Azygos anterior cerebral artery.

Figure 4

Typical time-frame images obtained from Gd-bolus tracking T_2*-weighted dynamic images (after the first injection). A white rectangle was placed in the MCA area (A), and its magnified images were visualized as (a), (b), (c), (d), and (e) in (B). TIC within the pixels is indicated by white arrows in (B), and the data were then plotted in a graph (C). Typical data points were extracted from the first injection at the times of

9.2 (a), 16.4 (b), 18.1 (c), 20.1 (d), and 33.9 (e) sec. In (A), the phase direction is shown as a white arrow.

Figure 5

TIC dynamic changes in the whole brain are shown in the first injection (A), the second injection (B), and the third injection (C). For each injection, a one-pixel ROI was selected and observed, as shown for the first (D), second (E) and third (F) injections, respectively. The negative enhancement changes in the rate from peak to base line on signal intensity were 16.8%(A), 10.0 %(B), and 10.3 %(C) at the whole brain (average 12.3, SD 3.9). The fraction of peak-to-base at selected ROIs were 19.2 %(D), 14.5 %(E), and 16.9 %(F) (average 16.9, SD 2.3), for the first, second, and third injections, respectively.

Figure 6

CBF maps using the AIF from MCA, pictured in a gray scale from 0 to 4 ml/g/min, in the first column on the left. MTT maps are shown in the next column, followed by the CBV maps with 0 to 2 ml/g/min in the third and last column. Deconvolution was carried out pixel by pixel with b-SVD and then smoothed to 0.15625×0.15625 mm in-plane resolution from acquired voxel resolution of a 0.625×0.625×3 mm (1.17 mm^3) in DSC-MRI.

Figure1
Click here to download high resolution image

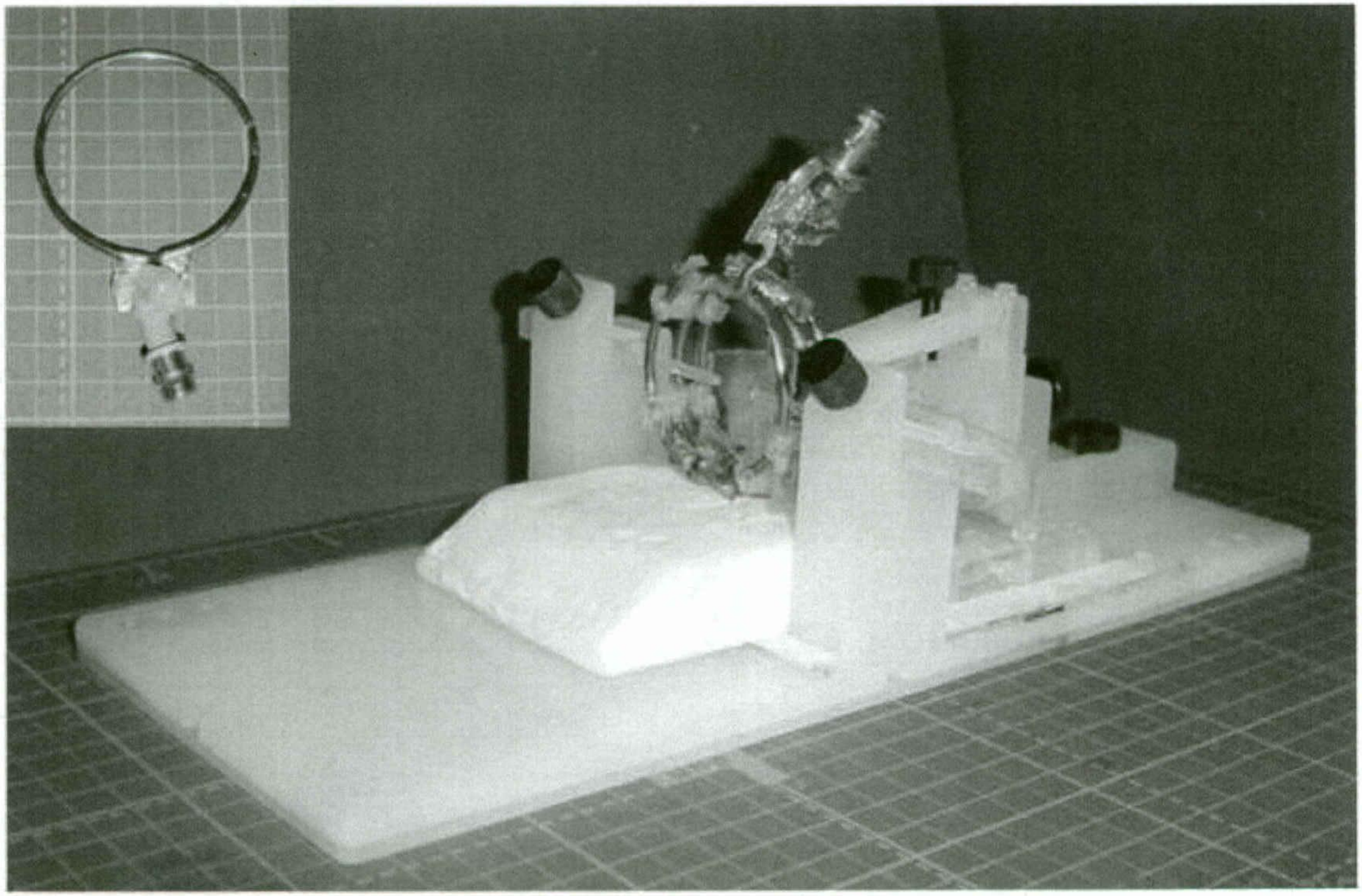

Figure2
Click here to download high resolution image

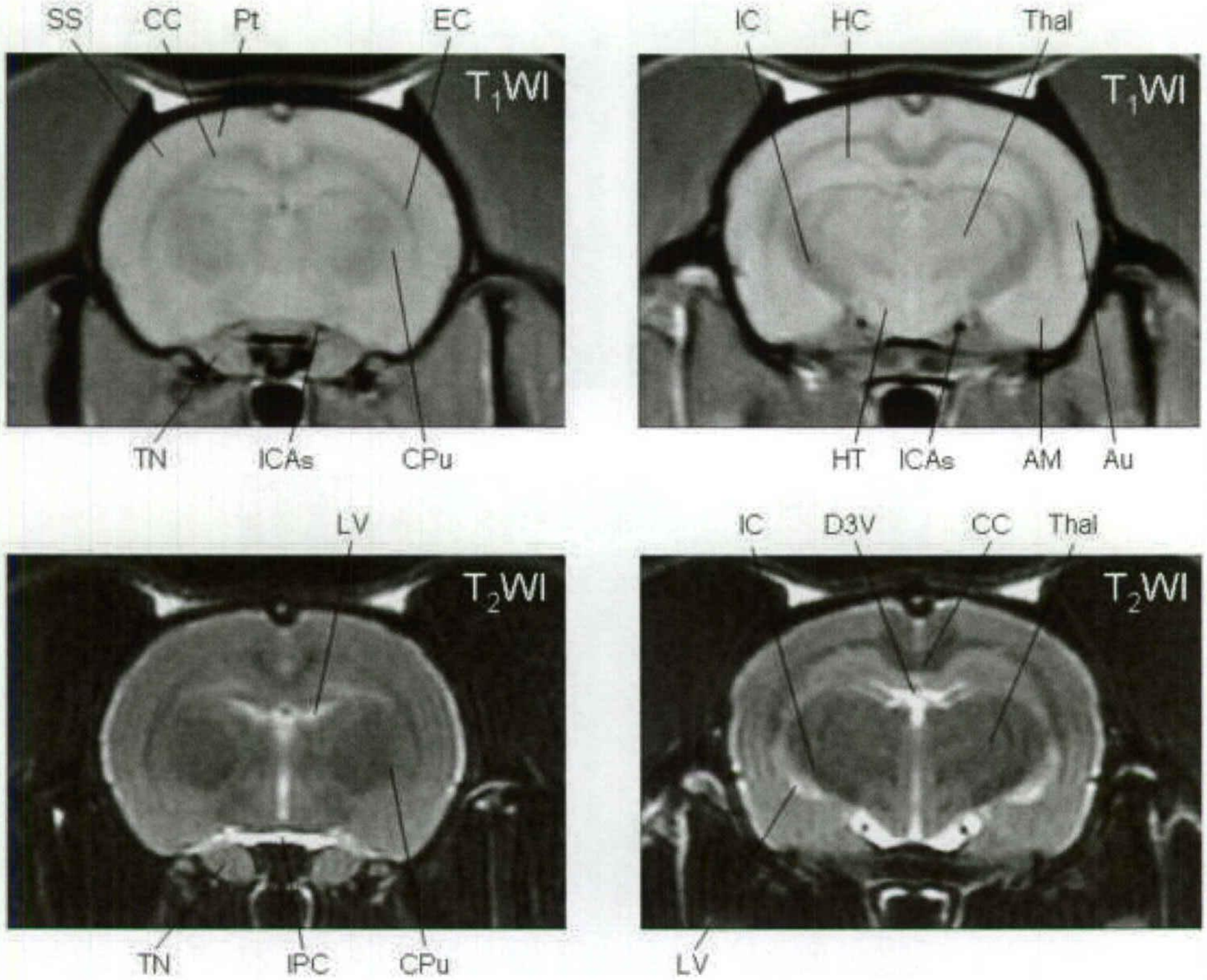

Figure3
Click here to download high resolution image

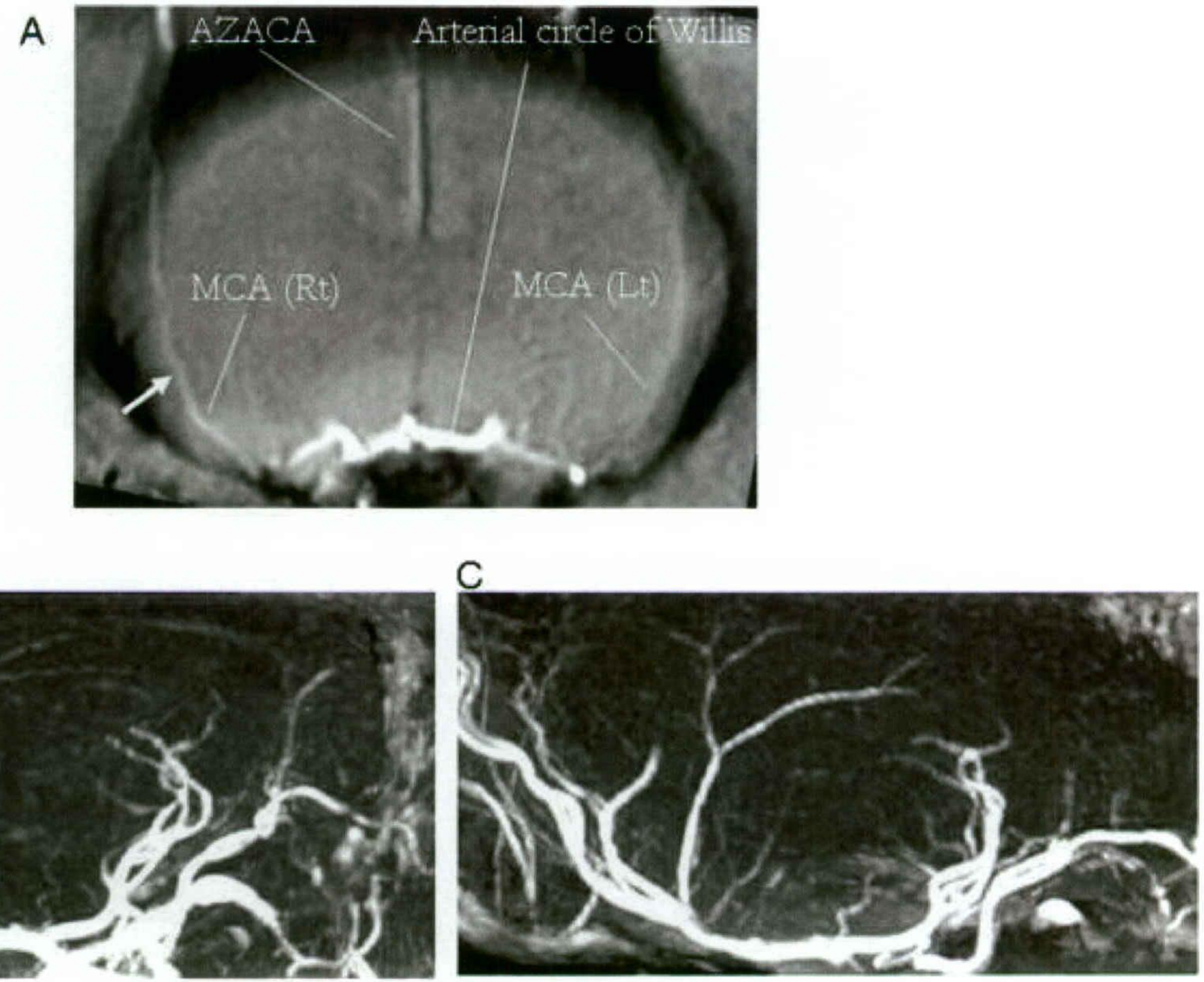

Figure4
Click here to download high resolution image

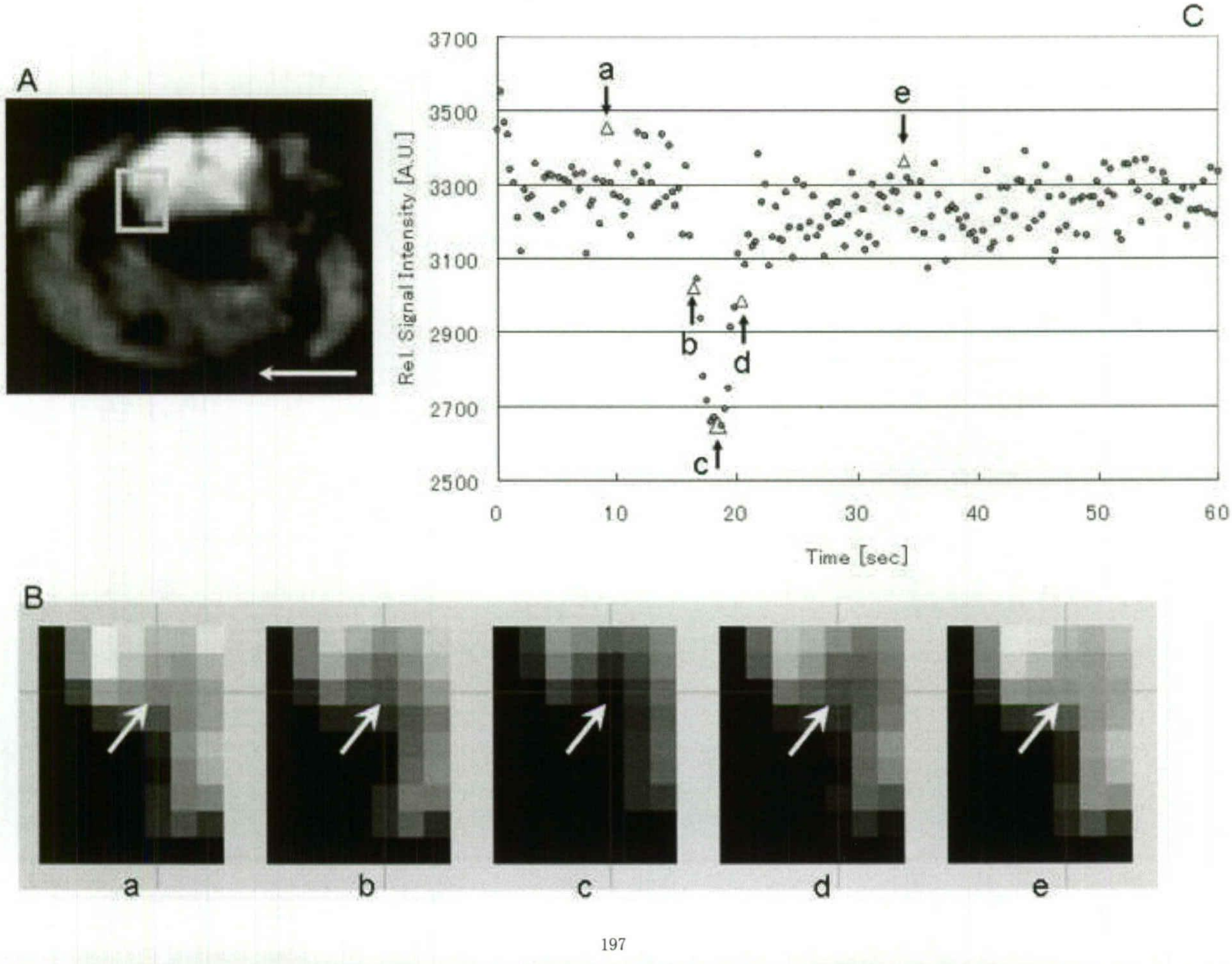

Figure5

Click here to download high resolution image

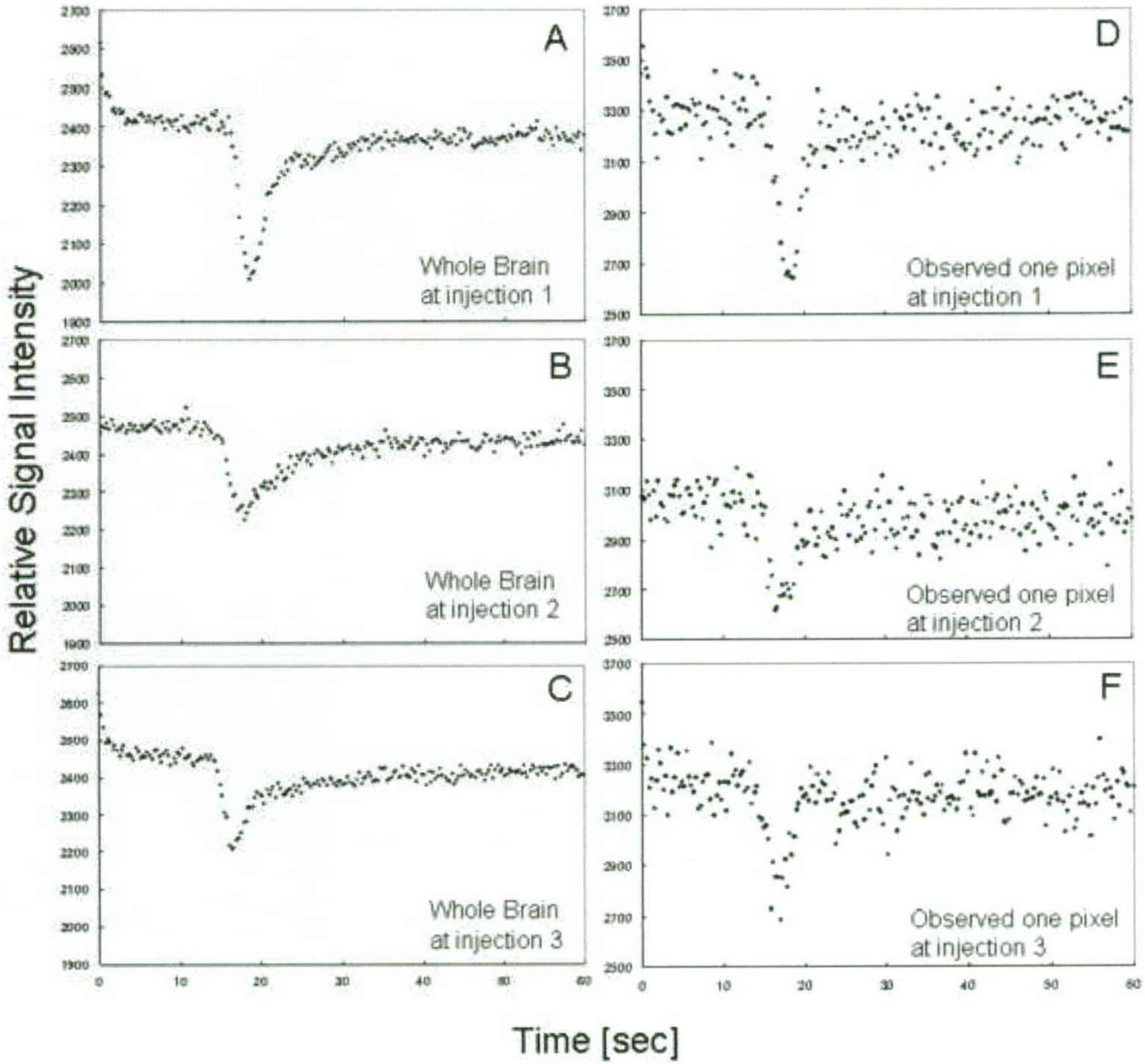

Click here to download high resolution image

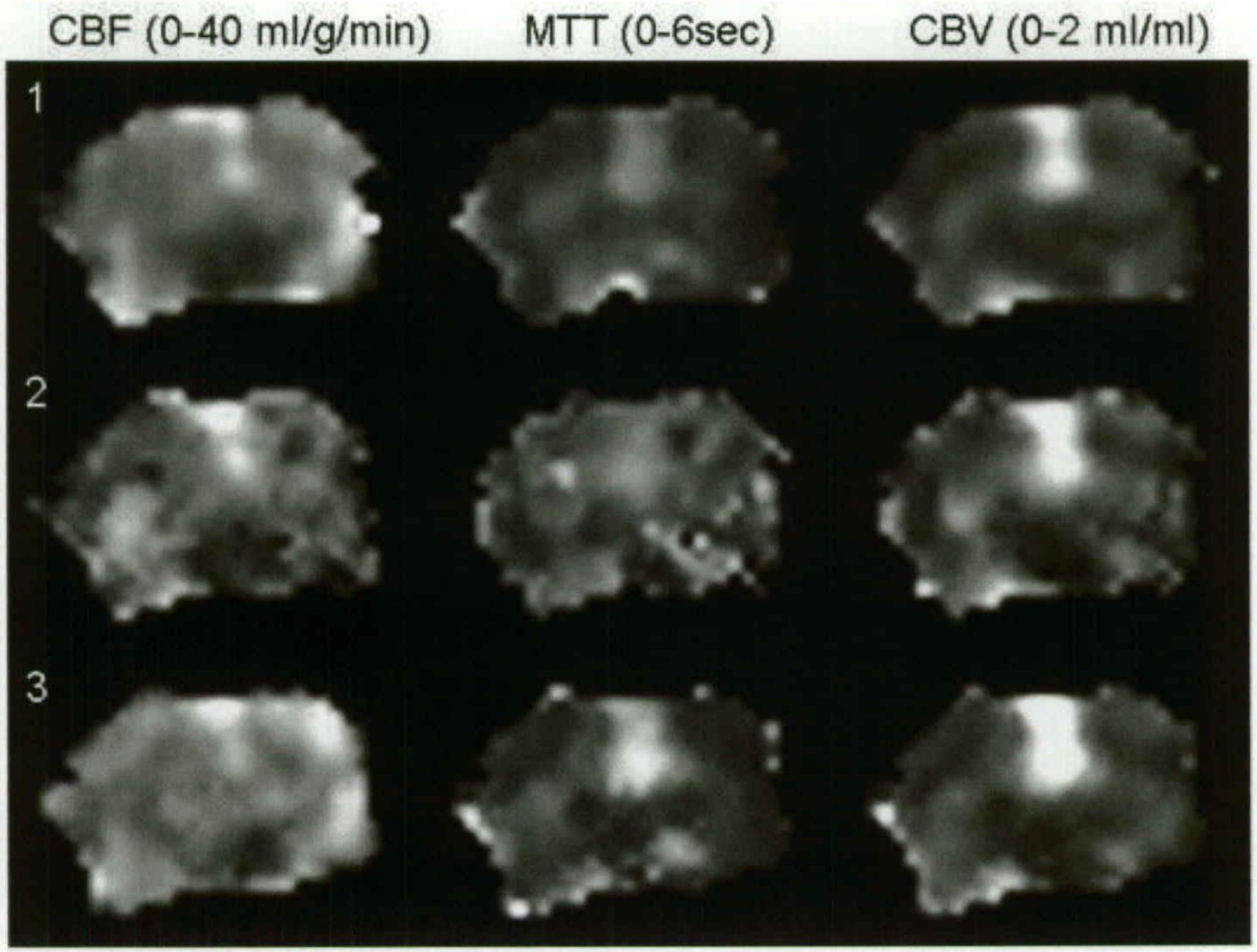

Journal of Cerebral Blood Flow & Metabolism (2008), 1–10

www.jcbfm.com

A physiologic model for recirculation water correction in $CMRO_2$ assessment with $^{15}O_2$ inhalation PET

Nobuyuki Kudomi, Takuya Hayashi, Hiroshi Watabe, Noboru Teramoto, Rishu Piao, Takayuki Ose, Kazuhiro Koshino, Youichirou Ohta and Hidehiro Iida

Department of Investigative Radiology, Advanced Medical-Engineering Center, National Cardiovascular Center Research Institute, Osaka, Japan

Cerebral metabolic rate of oxygen ($CMRO_2$) can be assessed quantitatively using $^{15}O_2$ and positron emission tomography. Determining the arterial input function is considered critical with regards to the separation of the metabolic product of $^{15}O_2$ (RW) from a measured whole blood. A mathematical formula based on physiologic model has been proposed to predict RW. This study was intended to verify the adequacy of that model and a simplified procedure applying that model for wide range of species and physiologic conditions. The formula consists of four parameters, including of a production rate of RW (*k*) corresponding to the total body oxidative metabolism ($BMRO_2$). Experiments were performed on 6 monkeys, 3 pigs, 12 rats, and 231 clinical patients, among which the monkeys were studied at varied physiologic conditions. The formula reproduced the observed RW. Greater *k* values were observed in smaller animals, whereas other parameters did not differ amongst species. The simulation showed $CMRO_2$ sensitive only to *k*, but not to others, suggesting that validity of determination of only *k* from a single blood sample. Also, *k* was correlated with $BMRO_2$, suggesting that *k* can be determined from $BMRO_2$. The present model and simplified procedure can be used to assess $CMRO_2$ for a wide range of conditions and species.
Journal of Cerebral Blood Flow & Metabolism advance online publication, 5 November 2008; doi:10.1038/jcbfm.2008.132

Keywords: arterial input; $CMRO_2$; mathematical modeling; recirculation water; PET

Introduction

Cerebral metabolic rate of oxygen ($CMRO_2$) can be quantitatively assessed using ^{15}O-labeled oxygen ($^{15}O_2$) and positron emission tomography (PET). This technique is based on an estimation of influx rate of $^{15}O_2$ to the cerebral tissue from arterial blood. Using information of cerebral blood flow (CBF) that may be obtained either from a separate scan with ^{15}O-labeled water ($H_2^{15}O$) or from the clearance rate $^{15}O_2$ of tissue, the oxygen extraction fraction (OEF) can also be calculated. The arterial input function must be determined before beginning this calculation. More specifically, a metabolic product of $^{15}O_2$ in the arterial blood, as a form of ^{15}O-labeled water (i.e., recirculating ^{15}O-water or RW) needs to be accurately estimated.

The arterial whole blood radioactivity curve can be obtained by measuring the radioactivity concentration of continuously withdrawn whole blood using a monitoring device (Eriksson *et al*, 1988; Eriksson and Kanno, 1991; Votaw and Shulman, 1998; Kudomi *et al*, 2003). Assessment of a time-dependent RW curve may be achieved by separating the plasma from the whole blood samples. This, however, requires labor-intensive procedures of frequent, manual arterial blood samplings, the centrifugation of all collected blood samples, and radioactivity measurements for both whole blood and plasma (Holden *et al*, 1988).

Ohta *et al* (1992) proposed to neglect the component of RW from the arterial input function. This technique fits three parameters of $CMRO_2$, CBF, and

Correspondence: Dr H Iida, Department of Investigative Radiology, Advanced Medical-Engineering Center, National Cardiovascular Center Research Institute, 5-7-1, Fujishirodai, Suita, Osaka 565-8565, Japan.
E-mail: iida@ri.ncvc.go.jp
This study was supported by the Program for Promotion of Fundamental Studies in Health Science of the Organization for Pharmaceutical Safety and Research of Japan, a Grant for Research on Advanced Medical Technology from the Ministry of Health, Labour and Welfare (MHLW), Japan, and by Nakatani Electronic Measuring Technology Association of Japan (NK).
Received 2 May 2005; revised 6 October 2008; accepted 11 October 2008

cerebral blood volume (CBV) to the kinetic $^{15}O_2$ data obtained from a single PET scan after the bolus administration of $^{15}O_2$. To minimize errors which result from neglecting RW, only the initial 3 mins of data after the bolus inhalation of $^{15}O_2$ were used when calculating the parameters. This approach has been applied to evaluate the magnitude of increase in $CMRO_2$ relative to that in CBF during cognitive stimulation tasks (Fujita *et al*, 1999; Vafaee and Gjedde, 2000; Okazawa *et al*, 2001*a*, *b*; Yamauchi *et al*, 2003; Mintun *et al*, 2002), but one of the drawbacks to this technique is the lack of accurate statistics, which is due to the use of a short scan duration.

Iida *et al* (1993) have developed a mathematical formula to predict the production of RW based on a physiologic model, which allows prolongation of the PET acquisition period with an additional statistical accuracy. The formula assumes a fixed rate constant for production of RW from $^{15}O_2$ in the body. This is based on the fact that the observed rate constant did not vary among clinical subjects, and thus causes nonsignificant errors in $CMRO_2$. However, the study is limited only to human subjects studied at rest, and results have not been verified using other species such as rat and mouse (Magata *et al*, 2003; Temma *et al*, 2006; Yee *et al*, 2006). Also, the findings have not been evaluated on humans who are under physiologic stress, though under such conditions the whole-body oxygen consumption is expected to change. Moreover, it is important to extend the approach to physiologically stressed conditions as recent progress for assessing $CMRO_2$ and CBF simultaneously from a short period dynamic scan by using a dual tracer autoradiography (DARG) (Kudomi *et al*, 2005). The DARG has enabled the $^{15}O_2$ PET to assess $CMRO_2$ and CBF simultaneously at various physiologically activated conditions.

The aim of this study is to verify the method used to estimate the arterial RW during the $^{15}O_2$ inhalation for simultaneous determination of $CMRO_2$ and CBF from the rapid procedures of $^{15}O_2$ PET. The feasibility of a simplified procedure is also being investigated. Applicability of this approach was tested for a wide range of species under various physiologic conditions. Experiments were designed to apply for different species as well as different physiologic conditions. A simulation study was also performed to evaluate the level of error sensitivity associated with this approach.

Materials and methods

Theory

Variables used in the recirculating water model are summarized in Table 1. The mathematical model that formulates the time-dependent RW in arterial blood consists of three rate constants: (1) the production rate of RW or k (per min), proportional to oxidative metabolism in the total body system ($BMRO_2$), (2) the forward diffusion rate (k_w, per min) of the metabolized ^{15}O-water between the blood and interstitial spaces in the body, and (3) the backward diffusion rate (k_2, per min) of the metabolized ^{15}O-water between the blood and interstitial spaces in the body. The differential equations for the arterial activity concentration of ^{15}O-water at a time t (secs) ($A_w(t)$, Bq/mL), after the physical decay correction can be expressed as follows (Huang *et al*, 1991):

$$\frac{d}{dt}A_w(t) = k \cdot A_o(t) - k_w \cdot A_w(t) + k_2 \cdot C(t) \quad (1a)$$

$$\frac{d}{dt}C(t) = k_w \cdot A_w(t) - k_2 \cdot C(t) \quad (1b)$$

$$A_t(t) = A_o(t) + A_w(t) \quad (1c)$$

where $A_o(t)$ and $A_t(t)$ denote the radioactivity concentration of the arterial $^{15}O_2$ and the total radioactivity from both

Table 1 Variables used in the recirculating water model

Symbol	*Description*	*Unit*
A_o	Radioactivity concentration of arterial $^{15}O_2$	Bq/mL
A_w	Radioactivity concentration of arterial $H_2^{15}O$	Bq/mL
A_t	Total radioactivity concentration from arterial $^{15}O_2$ and $H_2^{15}O$	Bq/mL
A_{plasma}	Radioactivity concentration of arterial plasma	Bq/mL
C	Activity concentration of $H_2^{15}O$ in peripheral tissue in a body	Bq/mL
Fi_{O_2}	Oxygen concentration in inhaled gas	%
Fe_{O_2}	Oxygen concentration in expired gas	%
k	Production rate of recirculating $H_2^{15}O$	per min
k_{BM}	Production rate of recirculating $H_2^{15}O$ obtained from BM approach	per min
k_w	Forward diffusion rate of $H_2^{15}O$ from blood to body interstitial space	per min
k_2	Backward diffusion rate of $H_2^{15}O$ from blood to body interstitial space	per min
λ	Decay constant of ^{15}O (= 0.00567 per sec)	per sec
v	Stroke volume	mL
p	k_w/k_2	
r	Respiration rate	per min
R	Fractional water content ratio in whole blood to that in the plasma	
R_{O_2}	Rate of oxidative metabolism in the whole-body system	mL/min
Δt	Delayed appearance time of recirculating water	secs
V_{O_2}	Total volume of molecular oxygen in total blood	mL
V_{TB}	Total volume of blood in a body	mL

$^{15}O_2$ and $H_2^{15}O$, respectively. $C(t)$ is an activity concentration of $H_2^{15}O$ in the peripheral tissue of the total body. Assuming a delayed appearance of RW by Δt (Iida *et al*, 1993), the following equation can be obtained:

$$A_w(t+\Delta t) = k(\alpha_1 \cdot A_t(t) \otimes \exp(-\beta_1 t) + \alpha_2 \cdot A_t(t) \otimes \exp(-\beta_2 t)) \quad (2)$$

where $\otimes$ denotes the convolution integral and:

$$\alpha_{1,2} = \frac{a - 2c \pm \sqrt{a^2 - 4b}}{\pm 2\sqrt{a^2 - 4b}}, \quad \beta_{1,2} = \frac{a \pm \sqrt{a^2 - 4b}}{2},$$
$$a = k + k_w + k_w/p, \quad b = k \cdot k_w/p, \quad c = k_w/p, \quad p = k_w/k_2 \quad (3)$$

Following four approaches were performed to determine the rate constants and $A_w(t)$.

Approach by four parameters fitting: Four parameters, k, Δt, k_w, and p ($=k_w/k_2$), can be determined from the observed RW ($A_w(t)$) and the $A_t(t)$ curves by means of the nonlinear least square fitting (4PF approach).

Approach by one parameter fitting: Once three parameters, Δt, k_w, and p, are fixed by averaging values determined by the 4PF approach, k can then be determined by fitting the Equation 2 to measured $A_w(t)$ from $A_t(t)$ (1PF approach). In this procedure, single datum is sufficient, and thus k can be determined from $A_t(t)$ and the RW counts sampled at a single time point.

Approach from steady-state condition: Similarly to the 1PF procedures, k can be determined from the steady state condition, which is achieved by a continuous administration of $^{15}O_2$ as follows (SS approach). Incorporating the decay constant of ^{15}O ($\lambda = 0.00567$ per secs) into Equations 1a and 1b provides:

$$\frac{d}{dt}A^*_w(t) = k \cdot A^*_o(t) - k_w \cdot A^*_w(t) + k_2 \cdot C^*(t) - \lambda \cdot A^*_w(t) \quad (4a)$$

$$\frac{d}{dt}C^*(t) = k_w \cdot A^*_w(t) - k_2 \cdot C^*(t) - \lambda \cdot C^*(t) \quad (4b)$$

where variables with the symbol * denote that no correction was made for the radioactivity decay of ^{15}O. After continuously administrating $^{15}O_2$, the radioactivity distribution of $A^*_o(t)$, $A^*_w(t)$, and $C^*_t(t)$ reaches a steady state. Thus, the following equations hold:

$$0 = k \cdot A^*_o(t) - k_w A^*_w(t) + k_2 C^*(t) - \lambda A^*_w(t) \quad (5a)$$

$$0 = k_w A^*_w(t) - k_2 C^*(t) - \lambda C^*(t) \quad (5b)$$

Given the values of k_w and k_2 which are determined as averages of 4PF, k can be calculated from the arterial $^{15}O_2$ and $H_2^{15}O$ concentrations at steady state as follows:

$$k = \lambda\left(\frac{k_w + k_2 + \lambda}{k_2 + \lambda}\right)\frac{A^*_w(t)}{A^*_o(t)} \quad (6)$$

Approach by the rate of whole body oxidative metabolism: In this study, an alternative approach is provided to obtain k, from the rate of oxidative metabolism in the whole-body system (BM approach). With this alternative approach, we assume that the production rate of RW or k is proportional to the rate of oxidative metabolism in the whole-body system (i.e., $BMRO_2$ (R_{O_2}, mL/min)). The rate of oxidative metabolism may change dependent on physiologic status of the subject. In addition, we assumed that this index can be defined from the difference of oxygen concentration between inhaled and exhaled trachea air samples. Therefore, the above can be expressed as follows:

$$k = c \cdot \frac{R_{O_2}}{V_{O_2}} \text{ (per min)} \quad (7a)$$

or

$$k_{BM} = \frac{k}{c} = \frac{R_{O_2}}{1.36 \cdot Hb \cdot V_{TB}} \quad (7b)$$

where c is the proportionality constant, k_{BM} the production rate of RW obtained from BM approach, V_{O_2} (mL) the total volume of molecular oxygen in total blood, 1.36 mL/g the amount of oxygen molecules combined with unit mass of hemoglobin, Hb (g/mL) represents the hemoglobin concentration in the arterial blood, and V_{TB} (mL) is the total volume of blood in the body.

Simulation

A series of simulation studies were performed to investigate the effects of errors on estimated $CMRO_2$ value in the model parameters (k, Δt, k_w, and p). In these simulations, a typical arterial blood time activity curve (TAC) of $^{15}O_2$ and $H_2^{15}O$ after DARG protocol (Kudomi *et al*, 2005) obtained in a monkey study was used. RW TACs were generated from the whole blood TAC by assuming baseline values of k as 0.13, 0.11, 0.34, and 0.73 per min, Δt as 20, 11, 5, and 3 secs, k_w as 0.38, 0.43, 0.98, and 0.87 per min, and p as 1.31, 1.01, 0.98, and 0.83, corresponding to humans, pigs, monkeys, and rats, respectively. Tissue TACs were generated by assuming CBF = 50 mL/min per 100 g and OEF = 0.4 ($CMRO_2$ was defined as: $CMRO_2 = CBF \times OEF \times C_aO_2$, where C_aO_2 is the arterial oxygen content. This simulation was intended to investigate magnitude of error as a percentage difference, so that arbitrary value of C_aO_2 was assumed) (Hayashi *et al*, 2003), using a kinetic formula for oxygen and water in the brain tissue (Mintun *et al*, 1984; Shidahara *et al*, 2002; Kudomi *et al*, 2005). $CMRO_2$ values were calculated by the DARG method (Kudomi *et al*, 2005), in which RW TACs were separated from the whole blood by changing k from 0.0 to 1.0 per min, Δt from 0 to 30 secs, k_w from 0.0 to 2.0 per min, and p from 0.0 to 2.0, respectively. Errors in the estimated $CMRO_2$ were presented as a percentage difference from the assumed true values.

Subjects

Subjects consisted of four groups including monkeys, pigs, rats, and clinical patients. Monkeys were six healthy *macaca fascicularis* with body weight of 5.2 ± 0.8 kg and age ranging from 3- to 4-year old. Pigs were three farm pigs

with body weight of 38 ± 9 kg and age from 4 to 12 months. Rats were 12 male Wistar rats with body weight of 300 ± 54 g and age from 7 to 8 weeks. All animals were studied during anesthesia. The animals were maintained and handled in accordance with guidelines for animal research on Human Care and Use of Laboratory Animals (Rockville, National Institute of Health/Office for Protection from Research Risks, 1996). The study protocol was approved by the Subcommittee for Laboratory Animal Welfare of National Cardiovascular Center.

Human data were retrospectively sampled from an existing database at National Cardiovascular Center which documented subjects who underwent PET examination after the ^{15}O-steady-state protocol. There were 231 total samples, with body weight and age ranging from 58 ± 10 kg, and 63 ± 14 years, respectively. Only the arterial $^{15}O_2$ and $H_2^{15}O$ radioactivity concentrations measured at the steady-state condition were used for the present analysis.

Experimental Protocol

The six monkeys were anesthetized using propofol (4 mg/kg/h) and vecuronium (0.05 mg/kg/h) assigned as a baseline in contrast to the after physiologically stimulated conditions. Animals were intubated and their respiration was controlled by an anesthetic ventilator (Cato, Drager, Germany). Each monkey inhaled 2,200 MBq $^{15}O_2$ for 20 secs. After 3 mins, the monkeys were injected with 370 MBq $H_2^{15}O$ for 30 secs by the anterior tibial vein. This was aimed at assessing both CBF and $CMRO_2$ according to the DARG technique (Kudomi *et al*, 2005). At 30 secs before inhaling $^{15}O_2$ to the monkeys, arterial blood was withdrawn from the femoral artery for 420 secs at a rate of 0.45 mL/min using a Harvard pump (Harvard Apparatus, Holliston, MA, USA). The whole blood TAC was measured with a continuous monitoring system (Kudomi *et al*, 2003) and the $A_r(t)$ was obtained. Meanwhile, we also manually obtained 0.5 mL of arterial blood samples from the contralateral femoral artery at 30, 50, 70, 90, 110, 130, 160, 190, and 360 secs after the $^{15}O_2$ inhalation. For the analysis of sampled blood, 0.2 mL of the blood were used for measurement of the radioactivity concentration of the whole blood, and the rest of the blood sampled (~0.3 mL) was immediately centrifuged for separation to measure the plasma radioactivity concentration ($A_{plasma}(t)$, Bq/mL). The radioactivity concentration was measured using a well counter (Molecular Imaging Laboratory Co. Ltd, Suita, Japan).

In two monkeys, anesthetic level was changed by altering the injection dose of propofol from 4 (baseline) to 8 and then to 12 and 16 mg/kg/h in one monkey, and to 5 and then to 7, 10, and 15 mg/kg/h in the other. In another monkey, $PaCO_2$ level was varied from 39 (baseline) to 47, and then to 33, 26, and 42 mm Hg by changing the respiratory rate. Each measurement for $^{15}O_2$ inhalation and $H_2^{15}O$ injection was initiated after at least 30 mins of applying the physiologic stimulation to achieve a steady state. All procedures were the same as those for the baseline, with the exception of the manual blood sample, which was obtained only once at 70 secs.

Before and after 6 mins of the $^{15}O_2$ inhalation, oxygen concentration in both inhaled (Fi_{O_2}, %) and end-tidal expiratory gas (Fe_{O_2}, %) was measured by the anesthetic ventilator in five out of the six monkeys. Using the respiration rate (r, per min) and the stroke volume (v, mL) indicated on the ventilator, the $BMRO_2$ (R_{O_2} mL/min) was calculated using the following equation:

$$R_{O_2} = (Fi_{O_2} - Fe_{O_2}) \cdot v \cdot r.$$

All monkeys received a PET measurement to assess the $CMRO_2$ at physiologically baseline condition. The scan protocol followed the DARG technique (Kudomi *et al*, 2005) in which a 6-mins single dynamic PET scan was performed in conjunction with the administration of dual tracers (i.e., $^{15}O_2$ followed by $H_2^{15}O$ after a 3-mins interval). PET scanner used was ECAT HR (Siemens-CTI, Knoxville, TN, USA), which provided 47 tomographic slice images for an axial field-of-view of approximately 150 mm. We performed arterial–sinus blood sampling to obtain a global OEF (OEF_{A-V}) (A–V difference approach). We sampled 0.2 mL of arterial and sinus blood simultaneously during each PET scan and measured their oxygen content (C_aO_2 and C_vO_2, respectively) (Kudomi *et al*, 2005). The OEF_{A-V} was calculated as: $OEF_{A-V} = (C_aO_2 - C_vO_2)/C_aO_2$.

With regards to the farm pigs involved in this experiment, we used existing data, which were originally obtained in one of the myocardial projects. During the study, three farm pigs were anesthetized. Anesthesia was induced by ketamine (10 mg/kg) and maintained using propofol (4 mg/kg/h). Animals were intubated and their respiration was controlled by the anesthetic ventilator. Venous blood was labeled with $^{15}O_2$ using a small artificial lung unit (Magata *et al*, 2003). $^{15}O_2$-labeled blood (222 to 700 MBq) was injected for 10 secs via anterior tibial vein. At 30 secs before this injection, arterial blood was withdrawn from the femoral artery at a rate of 0.45 mL/min using the Harvard pump and continued for 420 secs. The whole blood TAC ($A_r(t)$) was then measured with a continuous monitoring system (Kudomi *et al*, 2003). Meanwhile, we manually sampled 0.5 mL of arterial blood from the contralateral femoral artery at 30, 60, 90, 90, 120, 180, 240, and 300 secs after the $^{15}O_2$-labeled blood injection. For the analysis of sampled blood, 0.2 mL of the blood were used for measurement of the radioactivity concentration of the whole blood, and the rest of the blood sampled (~0.3 mL) was immediately centrifuged for separation to measure the plasma radioactivity ($A_{plasma}(t)$, Bq/mL). The radioactivity was measured using the well counter.

Data for rats were also originally obtained for other projects, and only the blood counts were used in this study. Anesthesia was induced with pentobarbital (50 mg/kg). A 10 mL of venous blood was labeled $^{15}O_2$ using a small artificial lung unit as described previously (Magata *et al*, 2003), and approximately 1 mL of $^{15}O_2$-labeled blood (37 to 74 MBq) was injected for 30 secs via the tail vein. Arterial blood samples of 0.1 mL each were obtained from the femoral artery at 5-secs intervals for 60 secs and 10-secs intervals for another 60 secs after the injection. Whole blood radioactivity concentration was measured using the well counter to be used as $A_r(t)$. Arterial blood samples of

0.2 mL each were obtained at 30, 60, 90, and 120 secs, and the plasma radioactivity concentration ($A_{plasma}(t)$) was measured by the well counter.

For clinical patients, the blood radioactivity concentration was obtained from previously performed PET examinations, which followed the steady-state protocol (Hirano *et al*, 1994). Each patient inhaled both $^{15}O_2$ and $C^{15}O_2$ to reach the steady state with an inhalation dose of approximately 1,200 and 500 MBq/min, respectively. Five to seven arterial blood samples were obtained during the steady state from the brachial artery. Mean values of radioactivity concentration of the whole blood and plasma, $A_t(t)$ and $A_{plasma}(t)$, respectively, were obtained for both $^{15}O_2$ and $C^{15}O_2$ PET examination.

Data Analysis

Using the blood activity data obtained from monkeys, pigs, and rats at baseline conditions, k as well as Δt, k_w and p were first determined by the 4PF approach, in which Equation 2 was applied to fit the $A_w(t)$ using the observed $A_t(t)$. Because the solubility of the oxygen is negligibly small in the plasma, we assumed that all radioactivity in plasma fraction comes from $H_2^{15}O$ and that the water content ratio of whole blood to plasma (R) does not change during measurement, which means that the kinetics of water molecules immediately reach equilibrium between the plasma and the cellular fraction (Mintun *et al*, 1984; Iida *et al*, 1993). Thus, $A_w(t)$ was obtained from the equation: $A_w(t) = A_{plasma}(t) \cdot R$, where R value was obtained from the sampled blood at the end of the scan (at which all the radioactivity in the blood can be considered as coming from $H_2^{15}O$ because inhaled $^{15}O_2$ is all metabolized).

Given that the values of Δt, k_w and p were averages determined from 4PF for monkeys, pigs, and rats, only k was determined by fitting Equation 2 to A_w. This was calculated at various points in time, more specifically, in 30, 50, 70, 90, 110, 130, 160, and 190 secs for monkeys, in 30, 60, 90, 90, 120, 180, and 240 secs for pigs, and in 30, 60, 90, and 120 secs for rats. The optimal time point for k under the 1PF approach was determined, so that $(k_{4PF}-k_{1PF})/k_{4PF}$ reaches a minimal value. Here, k_{4PF} and k_{1PF} denote k values determined by the 4PF and 1PF approaches, respectively. The values of k in monkeys at baseline condition, together with those in pigs and rats were compared between 4PF and 1PF approaches, in which a k value from the optimal single time point was used.

In three of the monkeys, which were physiologically stimulated, k of 1PF approach was obtained using single time point of A_w. Assuming the total blood volume (V_{TB}) for monkeys as 360 mL (Lindstedt and Schaeffer, 2002), and using Hb as measured value in each experiment, k_{BM} was calculated from R_{O_2} according to Equation 7b. Then, k_{BM} obtained as: $k_{BM} = 0.00204R_{O_2}$ was compared with k determined by 1PF.

For clinical data obtained from the steady-state (SS approach) PET examinations, Equation 6 was used to determine the k values of the SS approach for each patient, in which values of k_w and k_2 were 0.38 and 0.29 per min as obtained in a previous work by Huang *et al* (1991).

$CMRO_2$ and OEF values in monkeys at baseline condition were calculated using the RW TACs obtained by four different methods (i.e., directly measured $A_w(t)$ ($n = 6$), 4PF ($n = 6$), 1PF ($n = 6$), and BM approaches ($n = 5$)). Regions-of-interest were selected for over the whole brain, and $CMRO_2$ and OEF values were obtained in those regions-of-interest. The $CMRO_2$ values compared among the four methods mentioned above to estimate RW TACs. The Bland–Altman method was applied to analyze the agreement of OEF values between the methods. Also, OEF values were compared with OEF_{A-V}.

All data were presented as mean ± 1 standard deviation. Student's t-test was used and Pearson's regression analysis was applied to compare two variables. A probability value of <0.05 was considered statistically significant.

Results

Figure 1 shows results from the simulation study, and shows the magnitude of errors in $CMRO_2$ calculated by the DARG method as well as errors in the parameters, k, Δt, k_w, and p. Errors in $CMRO_2$ were most sensitive to errors in k amongst all species, namely the production rate constant of RW in the arterial blood. After errors in k, errors in $CMRO_2$ were sensitive to errors in Δt. Errors in k_w and p, however, appeared to cause relatively insignificant errors in $CMRO_2$. More specifically, only 5 to 10% errors are caused in $CMRO_2$ by a change of ± 50% in k_w and p.

Figures 2A–2C show examples of the arterial whole blood curves (A_t) and RW TAC (A_w) observed in typical studies on a monkey, a pig, and a rat, respectively. The RW curves became constant after a period in all species. The rise time or appearance of the RW curves, $A_w(t)$, was significantly delayed compare to that of whole blood curve, $A_t(t)$. $A_w(t)$ curves fitted by 4PF well reproduced the measured RW curves in three species: monkeys, pigs, and rats. Table 2 summarizes values of k, Δt, k_w, and p obtained by the four parameter fitting (4PF approach), at the baseline for monkeys, pigs, and rats, and also k value obtained by the steady-state formula for clinical patients. Those comparisons showed that the k was significantly different among species ($P < 0.001$) except between pig and human subjects, and it was significantly lower in smaller animals. Likewise, Δt showed significant differences among the three species ($P < 0.001$), and it was also lower in smaller animals.

Table 3 summarizes k and $CMRO_2$ values obtained from a series of PET experiments performed on six monkeys at baseline condition, and for increased anesthesia (in two monkeys), and changed $PaCO_2$ levels (in one monkey). The best agreement of k values between 4PF and 1PF approaches was obtained from the blood sample data taken at 60, 70, and 60 secs in pigs, monkeys, and rats, respectively, and was used in the 1PF approach. With this

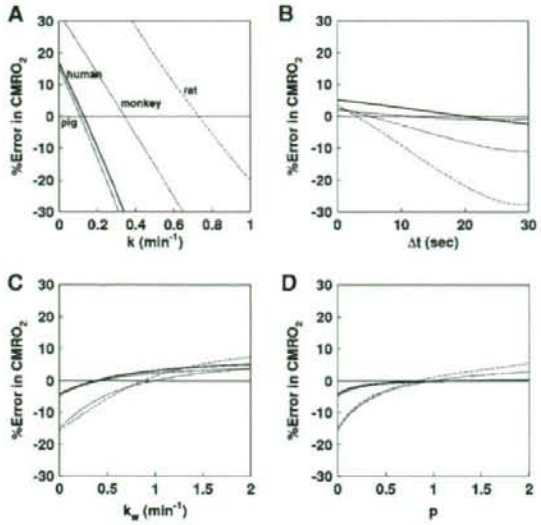

Figure 1 Error in $CMRO_2$ values due to errors in (**A**) k, (**B**) Δt, (**C**) k_w, and (**D**) p for assumed human, pig, monkey and rat. The same type of line indicates the same species. The percentage differences in the $CMRO_2$ values from the assumed true values (Table 1) were plotted as a function of the simulated value of k, Δt, k_w, and p.

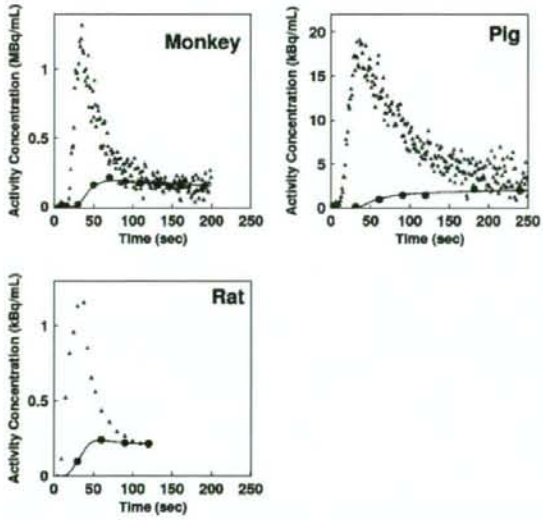

Figure 2 Representative comparison of the measured arterial whole blood and RW time activity curves for monkey, pig, and rat. Closed triangles and closed circles represent the measured whole blood and RW time activity curves, respectively. Estimated time activity curves by 4PF approach were also plotted in a solid line, and indicated a good agreement with the measured one.

optimized calibration protocol, k values were in a good agreement between 4PF and 1PF approaches. As shown in Figure 3, the regression analysis showed significant correlation for 21 animals including 6 monkeys, 3 pigs, and 12 rats ($P<0.001$), and there was no significant difference between the two variables. Figure 4 shows that k values calculated by the 1PF approach (at an optimized time) were in a good agreement with those calculated with the $BMRO_2$. Namely, the regression analysis showed significant correlation ($P<0.001$, $n=16$) and also that there was no significant difference between the two variables. Note that, in the $CMRO_2$ calculation by $BMRO_2$, k values were normalized according to the regression line shown in Figure 4. It should also be noted that calculated $CMRO_2$ values at the baseline shown in Table 3 were not significantly different among the four techniques. The average ($\pm$s.d.) values of obtained OEF were 0.53 ± 0.08, 0.52 ± 0.09, 0.54 ± 0.08, 0.54 ± 0.09, and 0.56 ± 0.04 from A–V difference, directly RW measured approach, 4PF, 1PF, and BM approaches, respectively. The Bland–Altman analysis of OEF values between from A–V difference and from others showed small over/underestimation, that is., with bias $\pm$ s.d. of -0.02 ± 0.09, 0.01 ± 0.07, 0.01 ± 0.08, and 0.02 ± 0.09, by direct RW, 4PF, 1PF, and BM approaches, respectively. Neither of the current methods (direct RW, 4PF, 1PF, and BM) was significantly different from A–V difference approach.

Discussion

Our study showed that the mathematical formula based on the physiologic model that reproduced the time-dependent concentration of RW in the arterial blood after a short-period inhalation of $^{15}O_2$ is indeed adequate. Our approach also simplified the procedures for sequential assessment of RW in $^{15}O_2$ inhalation PET studies, although previous approaches required frequent blood samples and centrifuges of each arterial blood sample. The present approach is an extension of a previous study by Iida *et al* (1993) and Huang *et al* (1991). It is essential if one intends to apply the rapid $^{15}O_2$ PET technique (Kudomi *et al*, 2005) to pharmacologic and physiologic stress studies on a wide range of species. Because the PET acquisition period can be prolonged >3 mins, statistical accuracy can be significantly improved as compared with Ohta *et al* (1992) and other researchers (Fujita *et al*, 1999; Vafaee and Gjedde, 2000; Okazawa *et al*, 2001*a*, *b*; Yamauchi *et al*, 2003; Mintun *et al*, 2002), under which to avoid effects of RW, the data acquisition period was limited only to <3 mins (Meyer *et al*, 1987; Ohta *et al*, 1992).

The present RW formula consists of three rate parameters of the production rate of RW in the arterial blood (k), and the forward and backward diffusion rate constants of RW between the blood and the peripheral tissues. The k was presumed to correspond to the oxygen metabolism in the total body system, $BMRO_2$, and was in fact shown to be

Table 2 Averaged values of k, Δt, k_w, and p for monkeys, pigs, rat, and human subjects under baseline condition

	Weight (kg)	k *(per min)*	*Δt (secs)*	k_w *(per min)*	p
Monkey	5.2 ± 0.8^a	0.34 ± 0.16^a	4.5 ± 1.4^a	0.98 ± 0.48	0.98 ± 0.30
Pig	38 ± 9^a	$0.11 \pm 0.02^{a,b}$	10.8 ± 1.8^a	0.83 ± 0.19	1.01 ± 0.26
Rat	0.30 ± 0.054^a	0.73 ± 0.16^a	2.9 ± 1.7^a	0.87 ± 0.30	0.83 ± 0.32
Human	58 ± 10^a	$0.129 \pm 0.023^{a,b}$	—	—	—

Monkey: $n = 6$; pig: $n = 3$; rat: $n = 12$; and human: $n = 231$. Measured values were obtained by 4PF for monkey, pig, rats, whereas those for human were obtained using data in a steady-state method.

[a]Denotes $P < 0.001$ for other species.

[b]Denotes that the difference was not significant in k between pig and human subjects.

Table 3 Values of k and $CMRO_2$ in the whole brain region for monkeys under physiologically baseline and stimulated conditions

ID	*Condition*	k *(per min)*			*$CMRO_2$ (mL/min per 100 g)*			
		4PF	*1PF*	*$BMRO_2$*	*Reference*	*4PF*	*1PF*	*$BMRO_2$*
1	BL	0.36	0.42	—	3.7	3.7	3.6	—
2	BL	0.62	0.66	1.24	3.0	3.3	3.4	3.4
3	BL	0.32	0.39	0.83	3.0	3.1	3.0	2.9
	(Dose of propofol)							
4	BL	0.21	0.18	0.55	2.0	2.0	2.0	1.8
	8 mg/kg/h	—	0.30	0.69	—	—	—	—
	12 mg/kg/h	—	0.23	0.52	—	—	—	—
	16 mg/kg/h	—	0.16	0.40	—	—	—	—
5	BL	0.12	0.15	0.31	2.1	2.1	2.0	1.8
	5 mg/kg/h	—	0.15	0.32	—	—	—	—
	7 mg/kg/h	—	0.16	0.35	—	—	—	—
	10 mg/kg/h	—	0.18	0.36	—	—	—	—
	15 mg/kg/h	—	0.071	0.29	—	—	—	—
	($PaCO_2$ level)							
6	BL	0.43	0.46	0.95	2.8	3.1	3.0	3.3
	47 mm Hg	—	0.20	0.64	—	—	—	—
	33 mm Hg	—	0.21	0.46	—	—	—	—
	26 mm Hg	—	0.14	0.28	—	—	—	—
	42 mm Hg	—	0.33	0.82	—	—	—	—

4PF, four parameters fitting; 1PF, one parameter fitting; $BMRO_2$, total body metabolic rate of oxygen; BL, baseline condition.
Reference: RW TAC was obtained using measured RW data at a baseline condition in all monkeys ($n = 6$). No statistically significant differences were found in $CMRO_2$ between reference and other techniques.

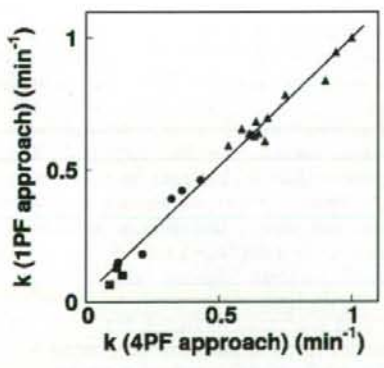

Figure 3 Comparison of the production rates of RW (k, per min) obtained by 4PF and those by 1PF. Squares, circles, and triangles correspond to pigs, monkeys, and rats, respectively. The regression line was $y = 0.97x + 0.026$ (per min) ($r = 0.98$).

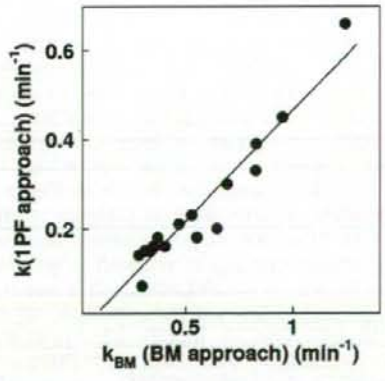

Figure 4 Comparison of the production rates of RW obtained by BM approach and those by 1PF approach in five monkeys at various anesthetic and $PaCO_2$ levels. The regression line was $y = 0.50x - 0.034$ (per min) ($r = 0.95$).